PHYSICA D

Devil-staircase behavior of dynamical invariants in chaotic scattering

Karol Życzkowski [a,b,*], Ying-Cheng Lai [c]

[a] *Centrum Fizyki Teoretycznej, Polska Akademia Nauk, Al. Lotników 32/44, 02-668 Warsaw, Poland*
[b] *Instytut Fizyki im. Smoluchowskiego, Uniwersytet Jagielloński, ul. Reymonta 4, 30-059 Kraków, Poland*
[c] *Departments of Mathematics and Electrical Engineering, Center for Systems Science and Engineering, Arizona State University, Tempe, AZ 85287-1804, USA*

Abstract

A crisis in chaotic scattering is characterized by the merging of two or more nonattracting chaotic saddles. The fractal dimension of the resulting chaotic saddle increases through the crisis. We present a rigorous analysis for the behavior of dynamical invariants associated with chaotic scattering by utilizing a representative model system that captures the essential dynamical features of crisis. Our analysis indicates that the fractal dimension and other dynamical invariants are a devil-staircase type of function of the system parameter. Our results can also provide insight for similar devil-staircase behaviors observed in the parametric evolution of chaotic saddles of general dissipative dynamical systems and in communicating with chaos. © 2000 Elsevier Science B.V. All rights reserved.

PACS: 05.45.+b; 47.52.+j

Keywords: Chaotic scattering; Dynamical invariants; Devil staircase

1. Introduction

Chaotic scattering is a manifestation of transient chaos [1,39] in classical open Hamiltonian systems. There has been a continuous interest in the subject [2,40]. A commonly utilized tool to quantify a classical scattering process is scattering functions, which are plots of some output variables characterizing the particle trajectory after the scattering versus some input variables characterizing the trajectory before the scattering. When the scattering is chaotic, a scattering function typically exhibits a fractal (Cantor) set of singularities. In the vicinity of each singularity, a small change in the input variable can result in a large change in the output variable — the signature of chaos. It is now known that the dynamical origin of chaotic scattering is nonattracting chaotic saddles in the phase space that contains an infinite number of unstable periodic and aperiodic orbits [1,2,39,40]. A trajectory coming into the scattering region typically spends a finite amount of time near the chaotic saddle before exiting the system. Staying near the chaotic saddle gives rise to the chaotic nature of the scattering process, and the set of infinite number of

---

* Corresponding author.

unstable periodic and aperiodic orbits embedded in the chaotic saddle leads to the infinite number of singularities in the scattering function. Chaotic scattering has been identified in models of different physical contexts such as chemical reactions [3,41], fluid dynamics [4,42–47], astrophysics [5,48,49], and atomic physics [6,50,51], etc.

A central question in the study of chaotic scattering is how chaotic scattering arises and evolves as a system parameter changes. Previous work has indicated that there are two routes to chaotic scattering: (1) the abrupt bifurcation route in which a chaotic saddle is suddenly formed in the phase space [7,52]; and (2) the period-doubling bifurcation route through which a chaotic saddle is gradually formed from a saddle-center bifurcation [8]. After onset of chaotic scattering, the underlying chaotic saddle can go through further evolution, leading to qualitative changes in the scattering characteristics. One example is the so-called massive bifurcation [9] in which an infinite number of unstable periodic orbits in the chaotic invariant set is suddenly destroyed and simultaneously replaced by another distinct class of infinite number of unstable periodic orbits. More recently, the phenomenon of *crisis in chaotic scattering* was discovered and studied [10–12] in which two previously existing chaotic saddles collide with each other via a complicated sequence of intersections of their stable and unstable manifolds. A physical consequence of crisis is that chaotic scattering is characteristically enhanced throughout the crisis in the sense that an infinite number of new possibilities for scattering trajectories are created due to tangencies of stable and unstable manifolds of the chaotic saddles. Dynamically, the fractal dimension of the chaotic saddle increases during the crisis. The aim of this paper is to provide a rigorous analysis for the behavior of dynamical invariants such as fractal dimension and topological entropy of the chaotic saddle during a crisis in chaotic scattering.

In [11,12], it was conjectured that the function of the fractal dimension of the chaotic saddle versus a system parameter during the crisis exhibits a behavior that can be characterized as a *devil staircase*. Mathematically, a relation $h(p)$ is called a devil staircase if $h(p)$ increases only at a Cantor set of Lebesgue measure zero but otherwise remains constant. Let p be the bifurcation parameter, and let p_1 and p_2 be the parameter values that mark the beginning and end of the crisis, respectively, where $p_2 > p_1$. Let the values of the fractal dimension before the crisis ($p < p_1$) and after the crisis ($p > p_2$) be D_1 and D_2, respectively. It was then found [11,12] that typically, $D_2 > D_1$ and, furthermore, during the crisis ($p_1 \leq p \leq p_2$), the fractal dimension versus p is a nondecreasing, devil-staircase type of function. This conclusion was derived based on numerical evidence and qualitative arguments. The initial more rigorous analysis of the problem was presented in [13]. In this paper, we proceed in this direction and verify *analytically* the devil-staircase characteristics of the fractal dimension. Our analysis yields the conclusion that other dynamical invariants of the chaotic saddle, such as the topological entropy and the escape rate, also exhibit a devil-staircase behavior, a result that has not been reported previously. Our approach is to investigate a class of simple, one-dimensional models for which a rigorous calculation of the topological entropy or the fractal dimension of the underlying chaotic saddle is possible. To compute the dynamical invariants, we use two methods: (i) integrating over an invariant measure; and (ii) analyzing the transition matrix. Since our model is representative of dynamical processes that involve homoclinic or heteroclinic tangencies and crossings of stable and unstable manifolds of chaotic saddles, we believe that the devil-staircase structure of dynamical invariants is typical in a large number of dynamical phenomena that involve the parametric evolution of chaotic saddles.

Although the main motivation of our study comes from chaotic scattering, we wish to point out that our results can also account for the devil-staircase behavior of dynamical invariants observed in at least two problems: (1) the change of topological entropy of chaotic saddles after a crisis in dissipative systems [14,15,53,54]; and (2) the relation between channel capacity and noise resistance in communicating with chaos, the latter has been a topic of recent interest [16,17,55–59].

Evolution of chaotic saddles after crisis: Crisis in dissipative dynamical systems is an event that converts a chaotic attractor into a chaotic saddle [14,53] as a system parameter changes through a critical value. In a typical nonlinear system such as the Hénon map, a crisis is induced by the collision of a chaotic attractor with the boundary of its own basin. Since the attractor lies in the closure of its unstable manifold, and since the basin boundary is the stable

manifold of a saddle periodic orbit on the boundary, the collision can be characterized as a homoclinic or heteroclinic tangency. As the parameter increases further through the crisis, an infinite number of tangencies occurs because both the stable and unstable foliations of the chaotic saddle after the crisis possess a fractal structure. Consequently, the chaotic saddle evolves after the crisis. It was found numerically that the topological entropy of the chaotic saddle after crisis typically exhibited a devil-staircase type of nondecreasing behavior [15,54].

Channel capacity in communicating with chaos: It was demonstrated recently that a chaotic system can be manipulated, via arbitrarily small time-dependent perturbations, to generate controlled chaotic orbits whose symbolic representation corresponds to the digital representation of a desirable message [16,55–58]. This idea has caught much attention partly because of one advantage of this type of digital-encoding strategy: the nonlinear chaotic oscillator that generates the waveform for transmission can remain simple and efficient, while all the necessary electronics controlling encoding of the signal remain at low-powered microelectronic level. A central issue in any digital communication devices is to select a proper coding scheme by which arbitrary messages can be encoded into the transmitting signal. It was argued that in general, a coding scheme generates chaotic trajectories that live on one of the infinite number of nonattracting chaotic saddles embedded in the chaotic attractor [17,59]. A relevant question is how much information the system can encode and transmit. A quantitative measure of the amount of information is the *channel capacity* [18,60], which is equivalent to the topological entropy [19] of the chaotic set utilized for encoding digital information. Since a coding scheme makes use of only an invariant subset embedded in the attractor, and since the topological entropy of the subset cannot be greater than that of the attractor, the channel capacity in any practical communication scheme employing a code must be less than or equal to that which would be produced in the ideal situation, where the full attractor is utilized for encoding messages. In [17,20,59], it was demonstrated that the function of the channel capacity versus a parameter characterizing the chaotic saddle as a consequence of coding typically exhibited a devil-staircase behavior.

The rest of the paper is organized as follows. In Section 2, we describe physical motivations from the perspective of chaotic scattering and introduce our analyzable model. In Section 3, we introduce the concept of integration over an invariant measure and apply it to our model system. In Section 4, we apply the method of transition matrix to compute dynamical invariants. In Section 5, we consider the issue of nonhyperbolicity and multifractality. In Section 6, we present a discussion.

2. Physical motivation and analyzable model

The physics that motivates us to consider the general phenomenon of interaction between nonattracting chaotic saddles is scattering. To give a specific example, consider the problem of particle scattering in a two-dimensional potential field consisting of an infinite array of elastic scatterers [10–12,21]. These scatterers are placed at constant intervals along, say, the y-axis. Each scatterer is represented by a circular attractive potential well, and there is no overlapping between adjacent potentials. The effect of each individual potential is to deflect the particle trajectory by an angle. This angle depends on the angular momentum of the particle with respect to the potential well with which it is interacting. Depending on the system parameters such as the particle energy, particles with slightly different initial angular momenta can exit the system at completely different locations and directions — signature of chaotic scattering. At relatively high energies, the deflection angles due to individual potentials are large enough to generate chaotic scattering, but they are still too small to cause a particle traveling upward near the $+y$-axis to reverse its direction to exit downward near the $-y$-axis, and vice versa. In this case, there are two isolated chaotic saddles in the phase space, corresponding to trajectories traveling upward and downward, respectively. As the particle energy is decreased, the maximum deflection angles increase so that a particle traveling upward can exit downward, and vice versa. Dynamically, this means that there is now an interaction between the previously two isolated chaotic saddles. The interaction begins when the stable (unstable) manifold of one chaotic saddle becomes

unstable foliations
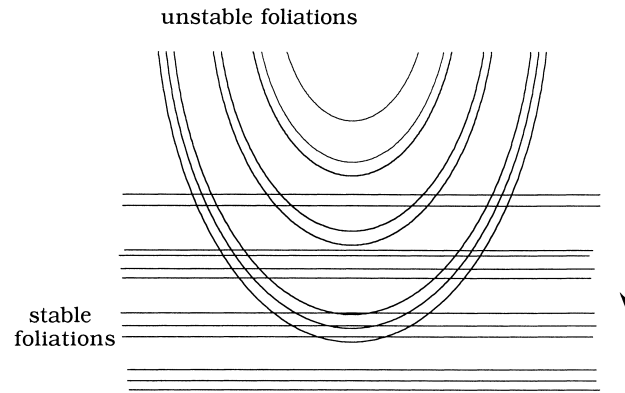
stable
foliations

Fig. 1. Schematic illustration of interaction between stable and unstable foliations of a chaotic saddle. Parametric evolution of the system corresponds to unstable foliations moving downwards.

tangent to the unstable (stable) manifold of another saddle. This marks the onset of a crisis. As the energy decreases further, an infinite number of tangencies occur. At another critical parameter value, no tangencies are possible, which corresponds to the end of the crisis. During the crisis, the fractal dimension of the conglomerated chaotic saddle increases whenever a new tangency occurs, leading to a devil-staircase behavior of the dimension and physically, to successive enhancement of chaotic scattering [12].

More precisely, the devil-staircase behavior can be seen as follows. Consider an invariant chaotic saddle in the two-dimensional plane. Since the saddle has a horseshoe-like structure, both the stable and unstable foliations are fractals, as shown schematically in Fig. 1, where the horizontal lines denote segments of the stable manifold and the curved ones are those of the unstable manifold. To characterize evolution of the saddle, assume that, as a system parameter changes, the unstable foliations move downwards across the stable foliations. At a generic parameter value, some unstable manifold becomes tangent to the stable one — a homoclinic or a heteroclinic tangency. Dynamically, an infinite number of unstable periodic orbits is created about such a tangency [22,61,62]. Thus, we expect the dynamical invariants, such as the topological entropy that measures the abundance of unstable periodic orbits, to increase abruptly at the tangencies. Due to the fractal structure of the stable and unstable foliations, such tangencies occur at a dense set of parameter values of Lebesgue measure zero. In any parameter subinterval, where there is no tangency, the dynamical invariants remain constant or change smoothly, since the topology of the stable and unstable manifolds remains unchanged. Overall, in a parameter interval containing both the first and last tangencies, we expect to see the values of dynamical invariants to increase abruptly at each tangency value, while they remain constant in any subinterval in between the tangency parameter values.

Crisis in chaotic scattering has also been observed in more realistic systems in atomic physics [23]. The essential ingredient characterizing this nonlinear phenomenon, which is independent of the physics of any specific model system, is the interaction between two or more previously isolated chaotic saddles. We thus seek to construct a model that captures this essential feature, yet the model should be simple enough, so that a rigorous understanding can be obtained. To the extent that the model is free of any feature specific to physical systems exhibiting crisis in chaotic scattering, we can regard predictions of the model as *universal* if they are also observed in numerical experiments of specific scattering systems. In particular, we consider the following one-dimensional model:

$$f(x) = \begin{cases} -a|x+1| + b & \text{for } x \le 0, \\ a|x-1| - b & \text{for } x > 0, \end{cases} \tag{1}$$

where $x \in \mathbf{R}$, and a and b are parameters ($b > -1$). The map is schematically shown in Fig. 2(a–d), where the four
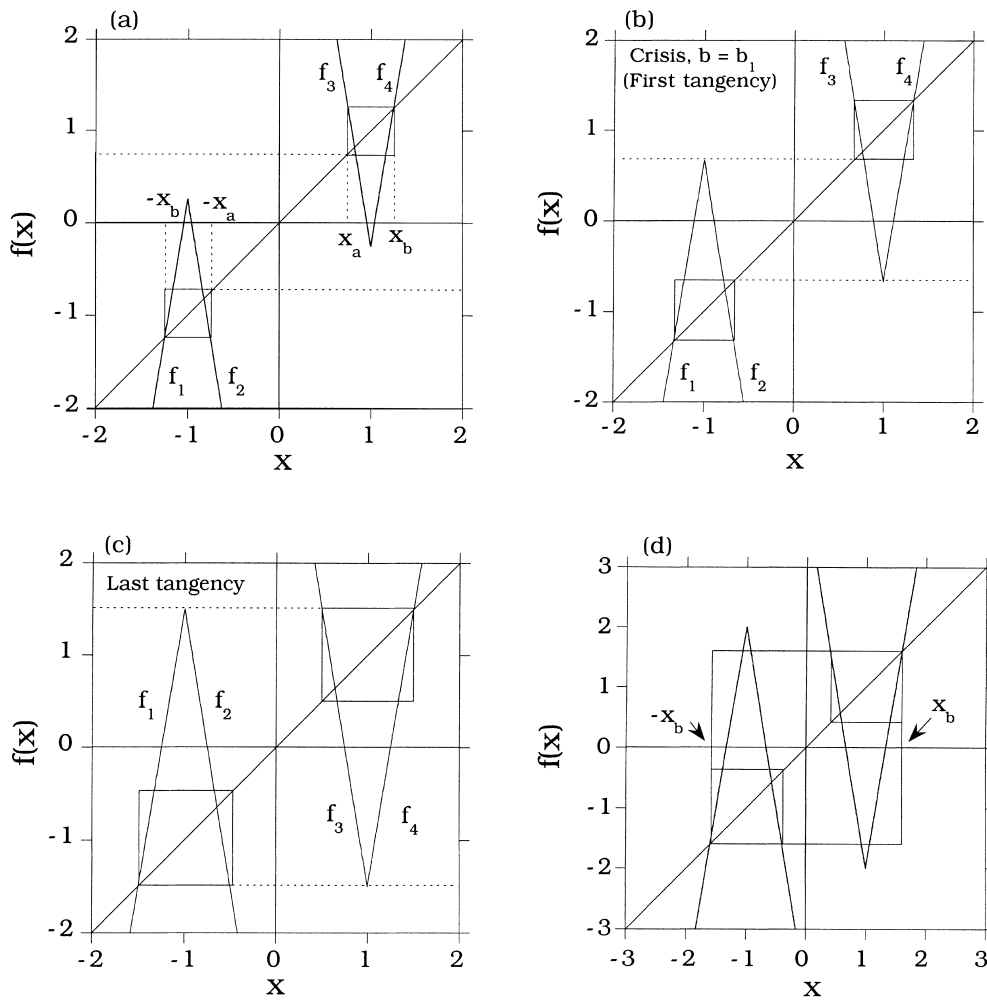
Fig. 2. Sketch of the model system (1) drawn for $a = 6$. The parameter a is kept constant, and the dependence of the dynamical properties of the system on the parameter $b \in [\frac{2}{3}, \frac{3}{2}]$ is investigated: (a) before crisis; (b) first tangency (beginning of crisis); (c) last tangency (end of crisis); and (d) after crisis.

branches of the map are labeled by $f_1(x)$ and $f_4(x)$ (positive slopes), and $f_2(x)$ and $f_3(x)$ (negative slopes). The map is invariant under the following symmetrical operations: $x \rightarrow -x$ and $f_b(x) \rightarrow -f_b(x)$. For small values of a, the map can exhibit bounded attractors, while for large a values, almost all initial conditions except a set of measure zero asymptote to either ∞ or $-\infty$. Since, we are interested in modeling a situation of scattering where particles eventually escape to $\pm\infty$, we fix a at a reasonably large value and investigate the dynamical behavior of the map as b is increased from zero. As shown in Fig. 2(a), there are two intervals: $A_+ \equiv [-x_b, -x_a]$ and $A_- \equiv [x_a, x_b]$, which are determined by the fixed points on the two branches of the map with positive slopes. For initial conditions outside these intervals, the resulting trajectories asymptote to either ∞ or $-\infty$ without entering the two intervals. The values of x_b and x_a are determined by the following relations: $a(x_b - 1) - b = x_b$ and $a(1 - x_a) - b = x_b$. We obtain

$$x_b = \frac{a+b}{a-1}, \qquad x_a = \frac{a-b-2}{a-1}. \tag{2}$$

To assure that almost all initial conditions asymptote to $\pm\infty$, we require that $x_a > 0$, or equivalently,

$$a \geq (b + 2). \tag{3}$$

Depending on the value of b, Eq. (1) exhibits different dynamical behaviors. In particular, when $f_b(1) > x_a$, there are attractors in the intervals A_+ and A_-. Initial conditions inside A_+ and A_- asymptote to the respective attractors. When $f_b(1) < x_a$, i.e., $a > 2$, almost all initial conditions in A_+ and A_- escape to ∞ except for two Cantor sets of Lebesgue measure zero. In this case, when one initial condition asymptotes to $+\infty$ (or $-\infty$), a slightly perturbed one may asymptote to $-\infty$ (or $+\infty$) and, hence, the dynamics are similar to those of chaotic scattering. When $f_b(1) > -x_a$, as shown in Fig. 2(a), the Cantor sets in A_+ and A_- are topologically and dynamically isolated. Trajectories resulting from initial conditions in A_+ cannot enter A_-, and vice versa. Due to symmetry, the fractal dimensions of these two Cantor sets are equal. To obtain the value of the dimension, we consider the interval A_+. At the first iteration, initial conditions in the interval $G_+ = (x_a + \delta, x_b - \delta)$ map outside A_+ and approach to either ∞ or $-\infty$ in subsequent iterations, where $\delta = 2(b + 1)/a(a - 1)$. Hence, there are two line segments of length δ that stay in A_+ after the first iteration. Two inverse images of G_+ on each side of G_+ map out of A_+ in two iterations and, hence, there are four intervals within A_+ of length δ/a that can stay in A_+ for two iterations. In general, there are 2^n intervals of length δ/a^{n-1} that can survive n iterations. Therefore, the box-counting dimension [24] of the Cantor set is

$$d_1 = -\lim_{n\to\infty} \frac{\ln 2^n}{\ln(\delta/a^{n-1})} = \frac{\ln 2}{\ln a}. \tag{4}$$

A crisis occurs when $f_b(+1) = -x_a$, or $b_1 = (a - 2)/a$, after which the two Cantor sets in A_+ and A_- are heteroclinically connected to each other, as shown in Fig. 2(b). This is a heteroclinic tangency analogous to that of stable and unstable manifolds in two-dimensional maps. As b increases beyond b_1, there can be an infinite number of such tangencies determined by the Nth iterated map $f_b^{(N)}(x) \equiv f_b(f_b(\ldots f_b(x)\ldots))$, where $N > 2$. The last tangency occurs when $f_b(+1) = -x_b$, or $b_2 = a/(a - 2)$, as shown in Fig. 2(c). For $b \geq b_2$, there is a single Cantor set in the interval $A_t \equiv [-x_b, x_b]$. The dimension of this Cantor set can be computed from Fig. 2(d). Initial conditions in $(-x_a, x_a)$ maps outside A_t in one iteration. In addition, there are open intervals $G_1 = (-x_b + \Delta, -x_a - \Delta)$ and $G_2 = (x_a + \Delta, x_b - \Delta)$ that maps outside A_t in one iteration, where $\Delta = 2(a + b)/[a(a - 1)]$. After the first iteration, there are four intervals of length Δ that survive in A_t for one iteration. The preimages of these four intervals consist of 16 subintervals of length Δ/a which stay in A_t for two iterations. In general, there are 4^n intervals of length Δ/a^{n-1} that survive in A_t for n iterations. Thus, the dimension of the Cantor set is

$$d_2 = -\lim_{n\to\infty} \frac{\ln 4^n}{\ln(\Delta/a^{n-1})} = 2\frac{\ln 2}{\ln a}. \tag{5}$$

Note that in order for d_2 to be less than 1, it is required that $a > 4$, otherwise $d_2 = 1$ and there will be attractors in A_t. The condition $a > 4$ is guaranteed by Eq. (2), which, when combined with $b_2 = a/(a - 2)$, gives the same constraint for a.

Eqs. (4) and (5) indicate that the fractal dimension of the Cantor set increases from d_1 to $d_2(= 2d_1)$ as b increases from values less than b_1 to values greater than b_2. The value of d, as we have seen above, is determined by the behavior of $f_b(x_c)$, where $x_c = \pm 1$ are the two critical points of the map. In [11,12], it was heuristically argued, based on examining the behaviors of higher iterates of the critical points, that for $b_1 < b < b_2$ (during the crisis), the fractal dimension increases from d_1 to d_2 in a manner that is typical of a devil staircase.

Note that the model equation (1) is piecewise linear and the absolute value of the derivative is constant: $|f'_b(x)| = a$ for any x. Hence, the natural invariant measure μ_* [25] covers uniformly the invariant set. Moreover, it coincides

with the Parry measure (maximal entropy measure) [1] and the Sinai–Ruelle–Bowen (SRB) measure [26,27]. Thus, the topological entropy h_T, the Kolmogorov–Sinai (KS) metric entropy h_{KS}, and the generalized Renyi entropies h_q of the system $f(x)$ are identical: $h_T = h_{KS} = h_q$. In an analogous way the constant slope of the map stipulates that the generalized dimensions (including the capacity D_0, the information dimension D_1, and the correlation dimension D_2 [24]) be all equal.

Our system is similar to the system analyzed by Bohr and Rand [26], in which a relation between the information dimension and the KS entropy is given as follows:

$$D_1 = \frac{h_{KS}}{\ln a}. \tag{6}$$

This relationship, which was first derived in [28] and corresponds to the Kaplan–Yorke conjecture [29], is also valid for our model. Thus, if the fractal dimension exhibits a devil-staircase behavior, so does the topological entropy, and vice versa.

For concreteness, in the analyses that follow, we fix $a = 6$ and choose b to be the bifurcation parameter, as in [11–13]. For this value of a, the *crisis* occurs for $b \in [b_1, b_2] = [\frac{2}{3}, \frac{3}{2}]$. Our aim is to provide a rigorous calculation for the behavior of the topological entropy and fractal dimension for b in this range.

3. Integration over fractal measures

The topological entropy of a chaotic system is the asymptotic rate of growth of the number of periodic orbits with respect to the length of the period [27]. Recently it was proposed that [20] for one-dimensional maps, the topological entropy can be computed by averaging the number of preimages with respect to the maximal entropy measure μ_* [27]. Consider a one-dimensional mixing system $f : X \to X$, where the function f is piecewise monotone and continuous on N branches. Its topological entropy is then given by [20],

$$h_T = \ln \int_X P(x) \, d\mu_*(x), \tag{7}$$

where $P(x) : X \to \{0, 1, 2, \ldots, N\}$ represents the number of preimages of f at the point x, restricted to the support of μ_*. For Eq. (1), there are only two preimages for $b < b_1$, which gives $h_T = \ln 2$. For $b > b_2$, there are four preimages so that the topological entropy is $h_T = 2 \ln 2$. Eq. (7) is also applicable to cases where $b \in (b_1, b_2)$, since the measure of maximal entropy μ_* is uniformly distributed over the invariant set and may be approximated by an iteration procedure. Fig. 3(a) shows the branches of the map in $x > 0$. To take into account the coupling with the left-side branch of the system, we use two auxiliary functions $f_5(x) = |f_3(x)|$ and $f_6(x) = |f_4(x)|$. Point b splits the invariant set S^+ into two parts: P_4 and P_2. For $x < b$ belonging to S^+, there exist four preimages, while for $x \in P_2$, there are only two. Making use of formula (7), we obtain

$$h_T = \ln \left[4 \int_{x_a}^{b} d\mu_*(x) + 2 \int_{b}^{x_b} d\mu_*(x) \right] = \ln 2 + \ln [1 + M], \tag{8}$$

where the relative weight M of the subset P_4 depends on b and is given by

$$M = \int_{x_a}^{b} d\mu_*(x). \tag{9}$$

---

[1] Maximal entropy measure of an invariant set is a measure that carries the same weight on each interval of the level-n coverage of the set, for any n. It is also the order zero Gibbs measure [1,26,39].
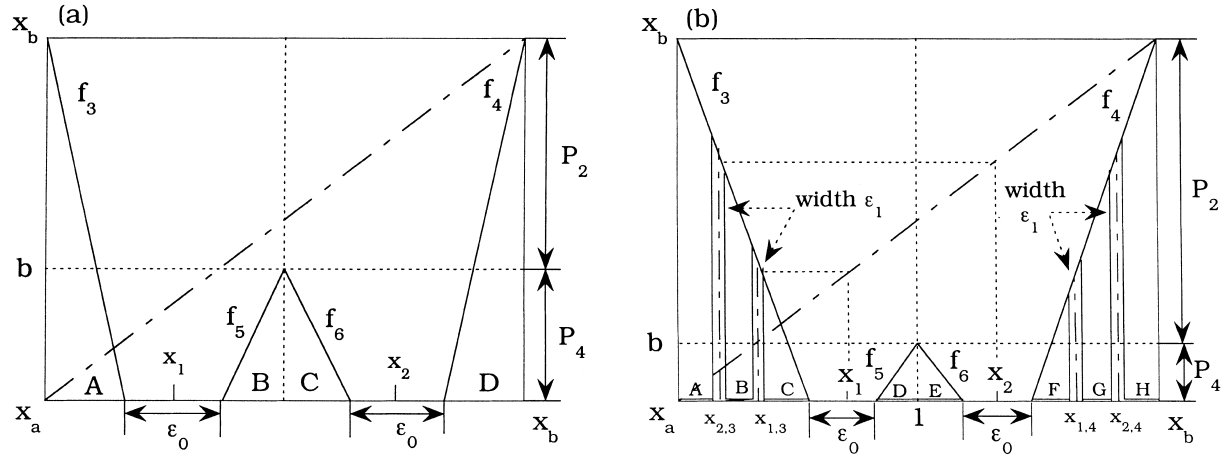
Fig. 3. (a) Right branch of the system. To describe the influence of the left branch of the system, we use auxiliary (nonexisting) functions f_5 and f_6. The points x_1 and x_2 are located at the centers of two primary gaps of the width ε_0. The support of the invariant set can be divided into two parts: P_4, for which each point has four preimages $f^{-1}(x)$, and P_2, for which there exist only two preimages. This figure is done for $b = b_1 = \frac{17}{18}$ and the dividing point b is located at the right edge of the gap g_1, which corresponds to the first primary dimension plateau of $D = \ln(1 + \sqrt{3})/\ln 6$. (b) For $b = b_{1,3} = \frac{30}{41}$, for which b is located at the point $x_{1,3}$. It is the preimage of the point x_1 with respect to the function $f_3(x)$ and is located in the center of the secondary gap of the width $\varepsilon_1 = \varepsilon_0/a$. In this case, we have the set P_4 consisting of two intervals $A \cup B$.

From Eq. (6), we obtain an *exact* result for the fractal dimension D of the chaotic saddle S for Eq. (1) at $a = 6$,

$$D = \frac{\ln 2 + \ln [1 + M]}{\ln 6}.\tag{10}$$

To compute the fractal dimension D, it is thus necessary to compute M, which can be obtained by successive approximations to the fractal measure $d\mu_*$. Since the map (1) is piecewise linear, the measure μ_* is distributed uniformly on the Cantor-like set S. To obtain the crudest (zeroth order) approximation $D^{(0)}$, we use the interval $S_0 \equiv [x_a, x_b]$ instead of the fractal set S^+. This is equivalent to using in Eq. (9) the Lebesgue measure dx in place of the fractal measure $d\mu_*$. The relative weight of P_4 is then approximated by the ratio $M^0(b) = (b - x_a)/(x_b - x_a)$, which, when substituted into Eq. (10), yields

$$D^{(0)}(b) = \begin{cases} \dfrac{\ln 2}{\ln 6} & \text{for } b < \frac{2}{3}, \\[2mm] \dfrac{\ln 2 + \ln [(4b - 1)/(b + 1)]}{\ln 6} & \text{for } b \in [\frac{2}{3}, \frac{3}{2}], \\[2mm] \dfrac{2 \ln 2}{\ln 6} & \text{for } b > \frac{3}{2}. \end{cases}\tag{11}$$

A better approximation is obtained by taking into account the two main gaps in the set S^+. These primary gaps g_1 and g_2 are determined by the points in which the functions f_3, f_5, f_6, and f_4 cross the line $y = x_a$. These gaps are centered at the points $x_1 = 1 - b/6$ and $x_2 = 1 + b/6$, and they have the width $\varepsilon_0 = \frac{1}{15}(4 - b)$. Note that both positions and widths of the gaps vary as b changes. Choosing a uniform measure on the set

$$S_1 := [x_a, x_b] \setminus [x_1 - \varepsilon_0/2, x_1 + \varepsilon_0/2] \setminus [x_2 - \varepsilon_0/2, x_2 + \varepsilon_0/2],$$

we obtain $M^{(1)}$, the first-order approximation of the integral equation (9). Substituting this integral into Eq. (11), we obtain the first-order approximation of the fractal dimension of the chaotic saddle

$$D^{(1)}(b) = \begin{cases} \dfrac{\ln 2}{\ln 6} & \text{for } b < 2/3, \\[2mm] \dfrac{\ln 2 + \ln [(13b - 7)/(4b - 1)]}{\ln 6} & \text{for } b \in [\frac{2}{3}, \frac{13}{17}], \\[2mm] \dfrac{\ln 2 + \ln [(9b - 1)/(8b - 2)]}{\ln 6} & \text{for } b \in [\frac{13}{17}, \frac{17}{18}], \\[2mm] \dfrac{\ln 2 + \ln [(27b - 18)/(8b - 2)]}{\ln 6} & \text{for } b \in [\frac{17}{18}, \frac{13}{12}], \\[2mm] \dfrac{\ln 2 + \ln [(15b - 5)/(8b - 2)]}{\ln 6} & \text{for } b \in [\frac{13}{12}, \frac{17}{13}], \\[2mm] \dfrac{\ln 2 + \ln [(14b - 11)/(4b - 1)]}{\ln 6} & \text{for } b \in [\frac{17}{13}, \frac{3}{2}], \\[2mm] \dfrac{2\ln 2}{\ln 6} & \text{for } b > \frac{3}{2}. \end{cases} \tag{12}$$

This function is not differentiable at six points for which the bifurcation parameter b coincides with the edges of the gaps g_1 and g_2. Every gap in the invariant fractal set S corresponds to a specific plateau in the function of $D(b)$, which is a devil staircase. To visualize this structure in a more transparent way, we show in Fig. 3(b) a more precise sketch of the invariant set S^+, in which the secondary gaps are indicated. These secondary gaps are the preimages of the primary gaps: $f^{-1}(g_1)$ and $f^{-1}(g_2)$. There are four secondary gaps for the value of b used in this graph; for larger values of b two or four new gaps appear in the central parts D and E. These secondary gaps have the width $\varepsilon_1 = \varepsilon_0/a$ and are centered at the preimages of the points x_1 and x_2. In Fig. 3(b), the symbol $x_{2,3}$ denotes the point $f_3^{-1}(x_2)$, etc. The set S_{i+1} can then be constructed by removing from S_i the preimages of all its gaps. Defining μ_i to be a uniform measure on the set S_i, we can compute the number

$$M^{(i)} = \frac{\int_{x_a}^{b} \mathrm{d}\mu_i}{\int_{x_a}^{x_b} \mathrm{d}\mu_i}.$$

The sequence of the measures μ_i converges in a weak sense to μ_*, so the sequence of integrals $M^{(i)}$ converges to M, defined as an integral over a fractal measure. A similar technique of computing dynamical entropies for various dynamical systems was discussed in [20,30,31].

Fig. 4 shows the dependence of the fractal dimension of the chaotic saddle S on the parameter b. Both approximations $D^{(0)}(b)$ and $D^{(1)}(b)$ are represented by the thin piecewise continuous lines. Due to a large contraction factor ($a = 6$), the convergence of $M^{(i)}$ is fast: the numerically obtained fifth-order approximation of the fractal dimension $D^{(5)}(b)$ (represented in the picture by a thick line) is already hardly distinguishable from the fourth-order one $D^{(4)}(b)$. Vertical lines indicate positions of the primary plateaus. Observe that the dependence $D(b)$ between them, say for $b \in (\frac{17}{13}, \frac{3}{2})$, is similar to the dependence in the entire interval (b_1, b_2). Formula (10) thus allows for a simple interpretation of the existence of the dimension plateaus, if the parameter b sweeps the gaps of the fractal set S, integral (9) remains constant, and so is the dimension D.
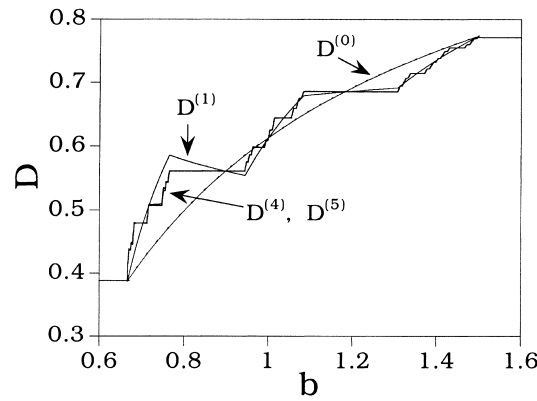
Fig. 4. Devil staircase of the fractal dimension D as a function of b. Narrow lines represent continuous approximations of $D^{(0)}(b)$ and $D^{(1)}(b)$, respectively, while the thick line represents $D^{(5)}(b)$. Points at the edges of the main dimension plateaus computed from the roots of the topological polynomials are collected in Table 1.

4. Method of transition matrix

For some values of the parameter b, the topological entropy of the chaotic saddle can be computed by identifying a Markov partition and constructing the Stefan transition matrix [32]. The entropy is given by the logarithm of the largest eigenvalue λ of the transition matrix [32–34]. Consider the special case $b_1 = \frac{17}{18}$, given by the solution of $f_5(b) = x_a$, as shown in Fig. 3(a). Note that this value of b marks the right end of the first primary dimension plateau. The primary gaps g_1 and g_2 divide the set S_0 into four parts: A, B, C, D. Let $A'B'C'$ and D' be the sets that are symmetric with respect to the origin, which are contained in the left part of the chaotic saddle S^-. These eight intervals form a Markov partition for the map f_{b_1}. Action of this map can be regarded as relations $A \rightarrow A \cup B \cup C \cup D$, $B \rightarrow A'$, $C \rightarrow A'$ and $D \rightarrow A \cup B \cup C \cup D$, where the arrow means that one set is mapped onto a union of others. These relations, together with four others that are symmetric to exchanging of the primes, lead to the following transition matrix:

$$
Q_1 = \begin{bmatrix}
1 & 1 & 1 & 1 & 0 & 0 & 0 & 0 \\
0 & 0 & 0 & 0 & 1 & 0 & 0 & 0 \\
0 & 0 & 0 & 0 & 1 & 0 & 0 & 0 \\
1 & 1 & 1 & 1 & 0 & 0 & 0 & 0 \\
0 & 0 & 0 & 0 & 1 & 1 & 1 & 1 \\
1 & 0 & 0 & 0 & 0 & 0 & 0 & 0 \\
1 & 0 & 0 & 0 & 0 & 0 & 0 & 0 \\
0 & 0 & 0 & 0 & 1 & 1 & 1 & 1
\end{bmatrix}.
\tag{13}
$$

The vectors are ordered as $\{A, B, C, D, A', B', C', D'\}$, while the nonzero entries represent the fact that one set is mapped by f onto the other one. The characteristic polynomial of Q_1 is

$$
W_1(z) = z^6(z^2 - 2z - 2),
\tag{14}
$$

where its largest root is $\lambda_1 = 1 + \sqrt{3}$. For convenience, we make use of the symmetry of the system f and identify the sets A and A'. Modifying relations $B \rightarrow A$ and $C \rightarrow A$ allows us to represent the same dynamics by the following smaller matrix:

$$Q'_{1+r} = \begin{bmatrix} 1 & 1 & 1 & 1 \\ 1 & r & r & 0 \\ 1 & r & r & 0 \\ 1 & 1 & 1 & 1 \end{bmatrix},$$

(15)

where $r = 0$. It is straightforward to check that λ_1 is its largest eigenvalue. Moreover, the matrix Q'_2 allows us to obtain the dimension for $b_2 \in [\frac{13}{12}, \frac{17}{13}]$, for which the upper limit of integral (9) sweeps across the other primary gap g_2. Such a case is described by $A \to A \cup B \cup C \cup D$, $B \to A \cup B \cup C$, $C \to A \cup B \cup C$, and $D \to A \cup B \cup C \cup D$, represented by the matrix Q'_{r+1} with $r = 1$. Its characteristic polynomial is $W_2(z) = z^2(z^2 - 2z - 2)$. The largest root of this topological polynomial, $\lambda_2 = 2 + \sqrt{2}$, determines the topological entropy $h_T = \ln(\lambda_2)$. Applying the relation (6), we obtain

$$D(b_1) = \frac{\ln(1 + \sqrt{3})}{\ln 6} \approx 0.5609305, \qquad D(b_2) = \frac{\ln(2 + \sqrt{2})}{\ln 6} \approx 0.6853303,$$

(16)

which agrees very well with the numerical data obtained in Section 3 and those in [11,12].

The same procedure can be applied to yield exact values for the dimension of the smaller plateaus corresponding to the secondary gaps centered at $x_{1,3}$. For example, consider the interval $b \in [\frac{103}{77}, \frac{107}{78}]$, as shown in Fig. 3(b). The allowed transitions are: $A \to F \cup G \cup H$, $B \to D \cup E$, $C \to A \cup B \cup C$, $D \to A \cup B$, $E \to A \cup B$, $F \to A \cup B \cup C$, $G \to D \cup E$, and $H \to F \cup G \cup H$; and the corresponding transition matrix is

$$Q_{1,3} = \begin{bmatrix} 0 & 0 & 0 & 0 & 0 & 1 & 1 & 1 \\ 0 & 0 & 0 & 1 & 1 & 0 & 0 & 0 \\ 1 & 1 & 1 & 0 & 0 & 0 & 0 & 0 \\ 1 & 1 & 0 & 0 & 0 & 0 & 0 & 0 \\ 1 & 1 & 0 & 0 & 0 & 0 & 0 & 0 \\ 1 & 1 & 1 & 0 & 0 & 0 & 0 & 0 \\ 0 & 0 & 0 & 1 & 1 & 0 & 0 & 0 \\ 0 & 0 & 0 & 0 & 0 & 1 & 1 & 1 \end{bmatrix}.$$

(17)

The largest root of the characteristic polynomial $W_{1,3}(z) = z^3 - 2z^2 - 2z + 2$ (denoted as $[1, -2, -2, 2]$), gives the exact value of the entropy h_T and the dimension D. Analytical results for each of the six secondary plateaus are collected in Table 1. Note that the topological polynomials contain even coefficients only. It is not difficult to find higher-order polynomials associated with the higher-order gaps in S and shorter stairs of the devil staircase $D(b)$. For example, the last third-order plateau corresponds to the polynomial $[1, -4, 0, 0, -2]$, which leads to the value of the dimension $D \approx 0.967988$.

We remark that another quantity characterizing nonattracting chaotic saddles, the decay rate κ [1,39], can be obtained in an analogous way. In particular, note that any trajectory starting with initial condition not belonging to the invariant set S escapes to infinity. Iterating the map f, on an initially uniform measure, causes the mass of points to decay exponentially in time: $\exp(-\kappa n)$. The relationship between decay rate κ and the topological entropy is shown by Tél [1,39] and Bohr and Rand [26],

$$\kappa = \ln a - h_{KS} = \ln 6 - \ln 2 - \ln[1 + M],$$

(18)

which can be obtained by estimating the integral M to various orders. Similar to the topological entropy and fractal dimension, κ versus b also exhibits a devil-staircase behavior.

Table 1

Fractal dimension of the repeller (1) at dimension plateaus with respect to variation of the parameter b. Subsequent columns contain, respectively, left and right edges of the plateaus, b_L and b_R, point x_i (or its preimage $x_i^{(j)}$ in the center of the gap labeling each plateau), topological polynomial[a], its largest root λ, integral M and the fractal dimension $D = \ln \lambda / \ln 6$

b_L	b_R	x_i	Polynomial	λ	M	D
$\frac{2}{3}$ (0.6667)	$\frac{2}{3}$ (0.6667)	b_1	$[1, -2]$	2.0	0.0	0.386852
$\frac{73}{107}$ (0.6822)	$\frac{77}{108}$ (0.7130)	$x_{2,3}$	$[1, -2, 0, -2]$	2.35930	0.17965	0.479063
$\frac{73}{102}$ (0.7157)	$\frac{77}{103}$ (0.7476)	$x_{1,3}$	$[1, -2, -2, 2]$	2.48119	0.24060	0.507177
$\frac{13}{17}$ (0.7647)	$\frac{17}{18}$ (0.9444)	x_1	$[1, -2, -2]$	2.73205	0.36602	0.560930
$\frac{103}{107}$ (0.9626)	$\frac{107}{108}$ (0.9907)	$x_{1,5}$	$[1, -2, -2, -2]$	2.91964	0.45982	0.597993
1 (1.0)	1 (1.0)	b_m	$[1, -3]$	3.0	0.5	0.613147
$\frac{73}{72}$ (1.0139)	$\frac{77}{73}$ (1.0548)	$x_{1,6}$	$[1, -4, 2, 2]$	3.17008	0.58504	0.643925
$\frac{13}{12}$ (1.0833)	$\frac{17}{13}$ (1.3077)	x_2	$[1, -4, 2]$	3.41421	0.70710	0.685330
$\frac{103}{77}$ (1.3377)	$\frac{107}{78}$ (1.3718)	$x_{1,4}$	$[1, -4, 2, -2]$	3.59867	0.79934	0.714697
$\frac{103}{72}$ (1.4305)	$\frac{107}{73}$ (1.4657)	$x_{2,4}$	$[1, -4, 0, 2]$	3.86620	0.93310	0.754717
$\frac{3}{2}$ (1.5)	$\frac{3}{2}$ (1.5)	b_2	$[1, -4]$	4.0	1.0	0.773705

[a] The symbol $[1, -2, -2]$ represents the polynomial $z^2 - 2z - 2 = 0$, whose root gives the topological entropy at the first primary plateau. For comparison, we added the values of b corresponding to the first, the middle and the last tangency, and marked by b_1, b_m and b_2, respectively.

5. Effect of nonhyperbolicity and multifractality

The analytic results in Sections 3 and 4 rely heavily on the fact that the model equation (1) is hyperbolic. In particular, the Lyapunov exponent of the chaotic saddle remains constant when the parameter b is varied so that $D_0 = D_1, h_T = h_{KS}$ and, consequently, it is possible to demonstrate, analytically, the devil-staircase behavior. To be more realistic, one has to consider the effect of nonhyperbolicity. Chaotic saddles in nonhyperbolic systems typically possess multifractality. In this case, $D_0 = D_1$ is no longer valid, and it is necessary to use the dimension spectrum D_q [35,63–65] to characterize the multifractality. Here we address the following question: does the devil-staircase behavior still persist when the dynamics is nonhyperbolic and multifractal? We are not able to answer this question analytically and, therefore, our approach will be to perform detailed numerical analyses using a class of nonhyperbolic maps.

We consider a class of maps derived from the analytic model equation (1) but the maps are no longer piecewise linear, which allows for nonhyperbolicity and multifractality. The map is given by [12]

$$g(x) = \begin{cases} -(2a + b)(x + 1)^2 + b, & x \le 0, \\ (2a + b)(x - 1)^2 - b, & x > 0, \end{cases} \tag{19}$$

where a and b are parameters. As in Eq. (1), we fix a and choose b as the bifurcation parameter. The map has two quadratic components in $x > 0$ and $x < 0$, respectively, and it has a local maximum at $x = -1$ and a local minimum at $x = +1$. As for Eq. (1), before crisis, there are two isolated chaotic saddles in $x > 0$ and $x < 0$, respectively. The first tangency occurs when the local maximum (minimum) at $x = -1$ ($+1$) touches the lower (upper) side of the square in which the chaotic saddle in $x > 0$ ($x < 0$) lies [cf. Fig. 2(b)]. This marks the beginning of the crisis. The last tangency, or the end of the crisis, occurs when the local maximum (minimum) at $x = -1$ ($+1$) touches the upper (lower) side of the square [cf. Fig. 2(c)]. The following relation determines the critical parameter values for the first and the last tangencies:

$$b = 1 \pm \left[\frac{1}{2(2a+b)} + \frac{\sqrt{(2a+b)(b+1) + \frac{1}{4}}}{2a+b} \right], \tag{20}$$

where the "−" and "+" signs are for b_c (the first tangency value) and b_f (the last tangency value), respectively.

Throughout our numerical experiments, we fix $a = 6$. It is found that $b_c \gtrsim 0.6$ and $b_f \approx 1.46$. We therefore choose the parameter interval $b \in [0.6, 2.0]$ and compute the various dynamical invariants of the chaotic saddles for 1000 values of b uniformly distributed in this interval. Specifically, we will compute: (1) the fractal dimensions D_q for $q = 0, 1, 2, 3$; (2) the Lyapunov exponent λ; (3) the escape rate κ; (4) the KS metric entropy h_{KS}; and (5) the topological entropy h_T. Our carefully controlled numerical computations reveal a devil-staircase-like behavior in all these dynamical quantities. In particular, at each tangency, all the dynamical invariants changes suddenly. However, unlike the piecewise linear system equation (1), all dynamical invariants, except for the topological entropy, no longer remain constant but change continuously in parameter subintervals between any two successive tangencies, as a result of change in the distribution of the natural measure. The topological entropy, on the other hand, remains constant in these parameter subintervals and, hence, its variation versus the system parameter is still a devil staircase. In what follows, we detail our computations.

5.1. Modified PIM-triple algorithm for computing continuous trajectories on the chaotic saddle

To compute various dynamical invariants, it is necessary to obtain a long, continuous trajectory on the chaotic saddle for each parameter value. We make use of the PIM-triple (proper interior maximum) algorithm [36], with significant modifications, to compute trajectories on the chaotic saddle. To see why modifications are necessary for our problem, we first briefly describe the algorithm. Given a parameter value, one selects an initial interval $[x_a, x_b]$, uniformly distributes N_{sub} points in the interval, and computes the lifetime T, i.e., the time during which the trajectory remains finite, for each point. One then selects three consecutive points $\{x_l, x_m, x_r\}$, or a triple, with the property that $T(x_m) > T(x_l), T(x_r)$. Because of this property, the triple is called a PIM-triple. One then lets $[x_a, x_b] = [x_l, x_r]$ and repeats the refining procedure until the size of the triple is very small, say, $(x_r - x_l) < \epsilon$. In so far as the triple is PIM, it contains points on the chaotic saddle. This is a refining process. To obtain a continuous trajectory on the chaotic saddle, the triple is iterated under the map, where if the size of the triple exceeds ϵ, the refining procedure is carried out. Iterating the triple, together with the refining process, can usually yield an approximate, arbitrarily long trajectory on the chaotic saddle [36]. The PIM-triple algorithm so described, as in [36], is suitable when the dynamical and topological properties of the saddle do not change appreciably in the parameter interval of interest. In our problem, however, these properties can change suddenly and drastically. We find, through trials and errors, that it is necessary to make the algorithm *adaptive* as the system parameter changes. Specifically, when the fractal dimensions are small, if the number N_{sub} of points utilized to search for PIM-triples is small, then it can occur that all N_{sub} points have the same lifetime and, hence, no PIM-triple can be found. On the other hand, if N_{sub} is large, then the computation becomes intense and even formidable. In our actual implementation, for a given parameter value, we start N_{sub} at a small value, say, 2^6. When a set of N_{sub} points fails to yield a PIM-triple, N_{sub} is increased by a factor of 2. The process is repeated until at least one PIM-triple is found. Usually, given an interval, several PIM-triples can be found, in which case we select the one with maximum difference in lifetimes $T_m - T_l$ and $T_m - T_r$. With these modifications, we find our algorithm can readily yield robust PIM-triple trajectories with more than 10^6 points, which is necessary for computing the various dynamical invariants. Because of the adaptivity, the computation is also efficient.
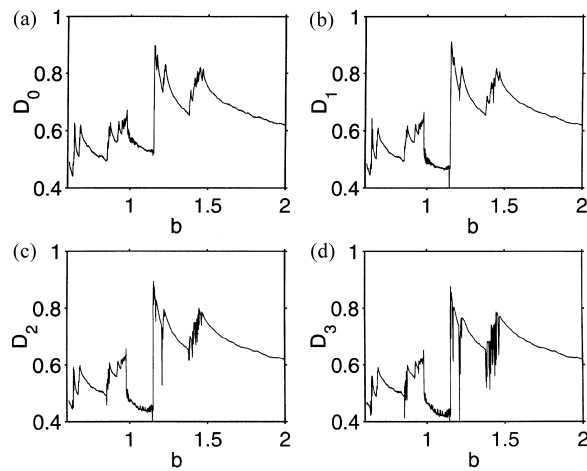
Fig. 5. (a–d) D_0, D_1, D_2, and D_3 versus b, respectively, for the nonhyperbolic quadratic map equation (19).

5.2. The dimension spectrum D_q

To define the fractal dimension spectrum, one utilizes a grid of boxes of size ϵ and compute the natural measure μ_i contained in each box. It is known that the PIM-triple algorithm can typically yield the natural measure of the chaotic saddle [37]. The dimension spectrum D_q is then defined as follows [35,63–65]:

$$D_q = \lim_{\epsilon \to 0} \frac{1}{q-1} \frac{\ln \sum_{i=1}^{K} \mu_i^q}{\ln \epsilon}, \tag{21}$$

where $K = K(\epsilon)$ is the total number of boxes with $\mu_i > 0$. The dimension spectrum D_q characterizes the fractal structure of the natural measure at different scales. In particular, smaller and smaller scales are characterized as q is increased. Amongst the infinite number of dimensions, D_0 is the box-counting dimension, D_1 is the information dimension, and D_2 is the correlation dimension. Generally, D_q is a nonincreasing function of q, i.e., $D_0 \geq D_1 \geq D_2$.

For the map equation (19), for each value of b, we compute a PIM-triple trajectory of 10^6 points. We then distribute a set of boxes in the interval $x \in [-2, 2]$ with box size ϵ ranging from e^{-11} to e^{-2}. The natural measure in each box is approximated by the frequency of visit of the PIM-triple trajectory to the box. The slopes of the linear fits of $\ln \sum_{i=1}^{K} \mu_i^q$ versus $\ln \epsilon$ give approximate values [2] of D_q. We find that the confidence interval of D_q is typically about 1% of the value of D_q. Fig. 5(a–d) show D_0, D_1, D_2, and D_3 versus b, respectively. Apparently, the values of these fractal dimensions change abruptly when a tangency occurs, and in the parameter subintervals between tangencies, they decrease continuously. These behaviors can be understood by examining the PIM-triple trajectories of the chaotic saddles. Fig. 6(a) and (b) show two PIM-triple trajectories, 50 000 points each, one before a tangency and another after for $b = 1.1516$ ($D_0 \approx 0.52$) and $b = 1.1530$ ($D_0 \approx 0.89$), respectively. We see that due to the tangency, the chaotic saddle suddenly acquires more pieces, leading to an abrupt increase in the fractal dimension. After the tangency, as b is increased further (but before the next tangency), the primary gap on the chaotic saddle widens continuously, resulting in a gradual decrease in the fractal dimensions. [3] In general, the curves of D_q's

---

[2] For the information dimension D_1, the fit is $\sum_i \mu_i \ln \mu_i$ versus $\ln \epsilon$.

[3] A similar situation occurs in the logistic map: $f(x) = rx(1 - x)$, where there is a chaotic saddle for $r > 4$ and its box-counting dimension decreases continuously as r varies further beyond.
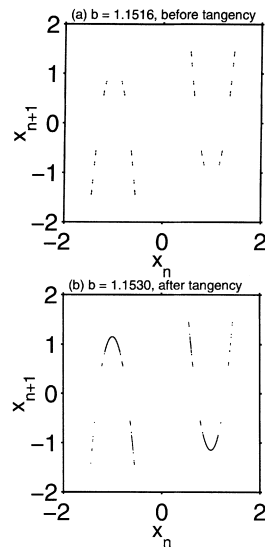
Fig. 6. For Eq. (19), PIM-triple trajectories of 50 000 points for: (a) $b = 1.1516$ ($D_0 \approx 0.52$, before a tangency), and (b) $b = 1.1530$ ($D_0 \approx 0.89$, after the tangency).

versus b contain an infinite number of sudden jumps caused by the infinite number of tangencies for $b \in [b_c, b_f]$. This behavior is typical of that of a devil staircase.

Note that for majority of the values of parameter b in Fig. 5(a–d), the dimensions satisfy $D_0 \geq D_1 \geq D_2 \geq D_3$. Nonetheless, there are a few parameter values for which these inequalities are violated by our numerical results. In particular, for about 1% of values of b, we actually observe that, e.g., D_0 is slightly less than D_1. This behavior occurs exclusively near tangencies about which the values of D_q tend to exhibit large fluctuations. The fluctuations are understandable because, near tangencies, we expect that the PIM-triple algorithm typically yields trajectories that less accurately represent the natural measure of the chaotic saddle. Such a numerical inaccuracy, however, does not affect the conclusion that the dimension spectrum exhibits a devil-staircase behavior.

5.3. The Kolmogorov–Sinai metric entropy h_{KS}

For chaotic saddles in one-dimensional maps, the KS metric entropy can be related to the Lyapunov exponent λ and the escape rate κ through the following relation [1,28,39]:

$$h_{KS} = \lambda - \kappa. \tag{22}$$

Since both λ and κ depend on the distribution of the natural measure, we expect these two quantities, and consequently the KS entropy, to exhibit a devil-staircase-like behavior similar to those of D_q's in Fig. 5(a–d). Fig. 7(a) shows λ versus b, where each value of λ is computed by using a PIM-triple trajectory of 10^6 points. In contrast to the behavior of the fractal dimensions, at each tangency, λ decreases abruptly, due to the sudden appearance of pieces of the chaotic saddle near the critical points $x = \pm 1$ which have near zero derivatives. In between the tangencies, λ increases because the gaps around the critical points widen, so that the average derivative of points on the chaotic saddle increases. To compute κ for each value of b, we distribute 10^7 initial conditions uniformly in the interval $x \in [-2, 2]$ and monitor the number $N(n)$ of trajectories that are still in the interval at time n. Typically, $N(n)$ decays exponentially: $N(n) \sim e^{-\kappa n}$, and the escape rate κ is obtained by a linear fitting of $\ln N(n)$ versus n. We
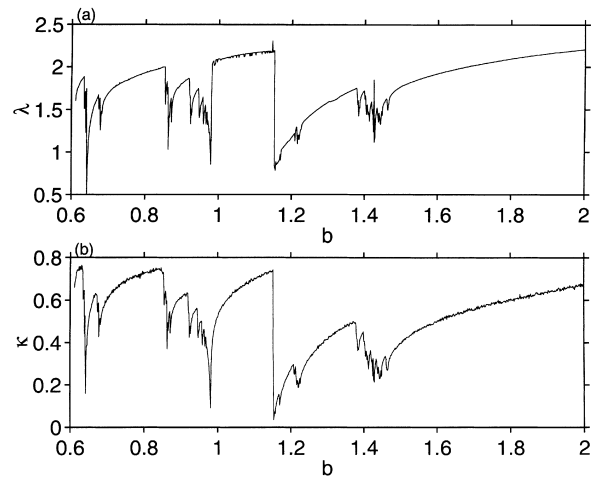
Fig. 7. (a) For Eq. (19), the Lyapunov exponent λ versus b, and (b) the escape rate κ versus b.

find that κ versus b exhibits a similar devil-staircase-like behavior as that of λ, as shown in Fig. 7(b). Fig. 8 shows the KS metric entropy versus b, which also exhibits a devil-staircase-like behavior.

5.4. The topological entropy h_T

Before the crisis, there are two isolated chaotic saddles, each is topologically similar to that in, say, the logistic map $f(x) = rx(1 - x)$ for $r > 4$. Thus, the topological entropy is $\ln 2$. After the last tangency, the chaotic saddles are connected and hyperbolic, as shown in Fig. 9. We see that the chaotic saddle is topologically equivalent to those in the piecewise linear model equation (1) after the crisis and, hence, we have $h_T = \ln 4$ for $b > b_f$. Thus, we expect h_T to increase during the crisis from $\ln 2$ to $\ln 4$. To numerically compute h_T, we utilize a simple counting method derived from the physical interpretation of the topological entropy: suppose a symbolic dynamics can be defined,
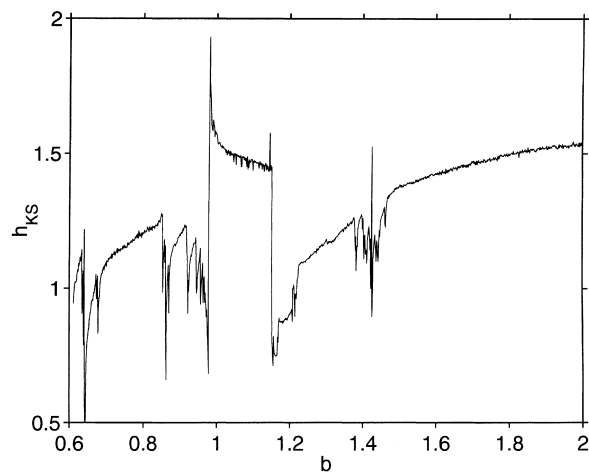
Fig. 8. For Eq. (19), the KS metric entropy h_{KS} versus b.
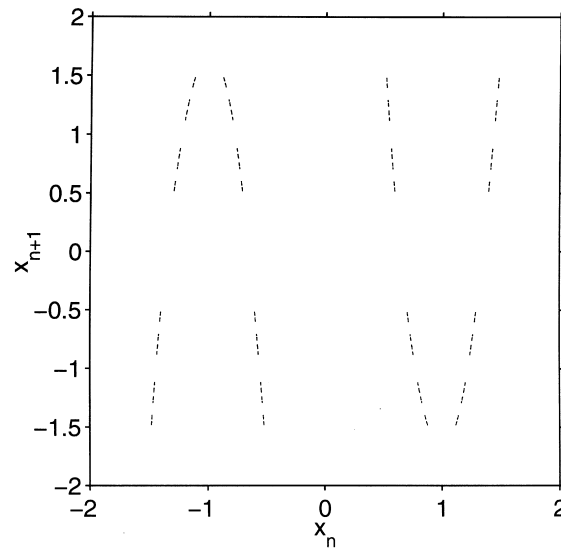
Fig. 9. A hyperbolic chaotic saddle with topological entropy $h_T = \ln 4$ after the crisis in Eq. (19) plotted for $b = 1.68$.

then a trajectory in the phase space $\{x_n\}_0^\infty$ corresponds to one in the symbolic space, denoted by $\{\sigma_n\}_0^\infty$, where σ takes on allowed symbols. The number N_n of distinct symbolic sequences of length n typically increases exponentially with n: $N_n \sim \exp(h_T n)$. Our model map equation (19) possesses two critical points and is discontinuous at $x = 0$, i.e., the map has four branches. Thus, four symbols are necessary for the symbolic dynamics. That is, each σ can take on four possible values, say, 0, 1, 2, and 3. In numerical experiments, n cannot be too large because the number of symbolic sequences can scale like 4^n. We use $n \leq 9$. Specifically, for each b value, we generate a PIM-triple trajectory of 4^{10} points, translate it into a trajectory in the symbolic space, and then count N_n. Typically, we find
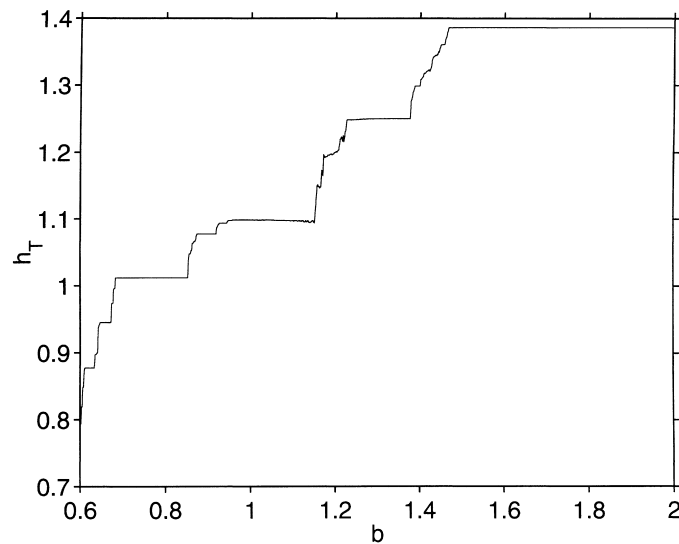
Fig. 10. For Eq. (19), the topological entropy h_T versus b. A nonmonotonic behavior visible around $b \approx 1.2$ is due to numerical artifacts.

that the slope of the linear fitting between $\ln N_n$ and n for $2 \leq n \leq 8$, which is approximately h_T, has a confidence interval that is at least two orders of magnitude smaller than the value of h_T itself, indicating that the computation of h_T is reliable. Fig. 10 shows h_T versus b, which is clearly a devil staircase, as h_T remains constants in between the jumps at which tangencies occur. This is consistent with our understanding that the topological changes in the chaotic saddle only occur at tangencies.

6. Discussions

The principal results of this paper are analytical and numerical confirmations for the devil-staircase behavior of dynamical invariants in crisis of chaotic scattering. For a class of hyperbolic maps, we make use of the concept of integration over a fractal measure and the transition matrix method to obtain analytically, to arbitrarily high-order approximations in principle, the fractal dimension and the topological entropy of the chaotic saddle going through a crisis. While the model that allows for such a treatment is a piecewise one-dimensional map, we argue that it captures the essential feature of chaotic scattering: interaction of chaotic saddles via an infinite number of tangencies between stable and unstable foliations. For nonhyperbolic maps, we perform carefully controlled numerical experiments which yield results that are similar to those obtained from the analyzable model. As such, we believe that the devil-staircase behavior of the fractal dimension or the topological entropy is a characteristic feature in physical phenomena that involves the parametric evolution of nonattracting chaotic saddles [38,66–68].

Our result has implications to communicating with chaos, a problem of recent interest. It was argued [17,59] that a coding scheme, which is necessary to encode a digital message into the waveform of a chaotic oscillator under the restriction of grammar of the dynamics, leads to trajectories that live on a chaotic saddle embedded in the chaotic attractor. Mathematically, this problem can be addressed as follows. Consider, say, the logistic map $x_{n+1} = rx_n(1 - x_n)$ for which the generating partition [28] for symbolic dynamics is the critical point $x_c = \frac{1}{2}$. Suppose we are interested in trajectories that never visit a small gap region of size s centered at x_c. The dynamical invariant set that supports such trajectories is a nonattracting chaotic saddle [17,59]. We ask, how does the topological entropy of the chaotic saddle depend on the gap size s? Noting that increasing the gap size is equivalent to removing preimages of the critical point (or tangencies), we see that the topological entropy must be a nonincreasing function of the gap size. Numerical evidence and analysis using transition matrices indicate that the topological entropy indeed follows a devil-staircase behavior [17,59]. In fact, the method of integration over a fractal measure can be employed to compute the topological entropy of chaotic saddles embedded in a chaotic attractor of piecewise linear maps [20].

References

[1] T. Tél, in: Bai-lin Hao (Ed.), Directions in Chaos, Vol. 3, World Scientific, Singapore, 1990.
[2] E. Ott, T. Tél, Chaos 3 (1993) 417.

[3] D.W. Noid, S. Gray, S.A. Rice, J. Chem. Phys. 84 (1986) 2649.
[4] B. Eckhardt, H. Aref, Trans. Soc. R. London A 326 (1988) 655.
[5] M. Hénon, Icarus 66 (1986) 536.
[6] B. Eckhardt, Europhys. Lett. 61 (1988) 329.
[7] S. Bleher, E. Ott, C. Grebogi, Phys. Rev. Lett. 63 (1989) 919.
[8] M. Ding, C. Grebogi, E. Ott, J.A. Yorke, Phys. Rev. A 42 (1990) 7025.
[9] M. Ding, C. Grebogi, E. Ott, J.A. Yorke, Phys. Lett. A 153 (1991) 21.
[10] G. Troll, Physica D 50 (1991) 276.
[11] Y.-C. Lai, C. Grebogi, R. Blümel, I. Kan, Phys. Rev. Lett. 71 (1993) 2212.
[12] Y.-C. Lai, C. Grebogi, Phys. Rev. E 49 (1994) 3761.
[13] Y.-C. Lai, K. Życzkowski, C. Grebogi, Phys. Rev. E 59 (1999) 5261.
[14] C. Grebogi, E. Ott, J.A. Yorke, Phys. Rev. Lett. 48 (1982) 1507.
[15] O. Biham, W. Wenzel, Phys. Rev. Lett. 63 (1989) 819.
[16] S. Hayes, C. Grebogi, E. Ott, Phys. Rev. Lett. 70 (1993) 3031.
[17] E. Bollt, Y.-C. Lai, C. Grebogi, Phys. Rev. Lett. 79 (1997) 3787.
[18] C.E. Shannon, W. Weaver, The Mathematical Theory of Communication, The University of Illinois Press, IL, 1964.
[19] R.C. Adler, A.C. Konheim, M.H. McAndrew, Trans. Am. Math. Soc. 114 (1965) 309.
[20] K. Życzkowski, E. Bollt, Physica D 132 (1999) 393.
[21] G. Troll, U. Smilansky, Physica D 35 (1989) 34.
[22] S. Newhouse, Publ. I. Hautes Etudes Sci. 50 (1979) 101.
[23] M. Toda, Phys. Rev. Lett. 74 (1995) 2670.
[24] J.D. Farmer, E. Ott, J.A. Yorke, Physica D 7 (1983) 153.
[25] J.-P. Eckmann, D. Ruelle, Rev. Mod. Phys. 57 (1985) 617.
[26] T. Bohr, D. Rand, Physica D 25 (1987) 387.
[27] A. Katok, B. Hasselblatt, Introduction to the Modern Theory of Dynamical Systems, Cambridge University Press, Cambridge, 1995.
[28] H. Kantz, P. Grassberger, Physica D 17 (1985) 75.
[29] J.L. Kaplan, J.A. Yorke, in: H.-O. Peitgen, H.-O. Walter (Eds.), Functional Differential Equations and Approximations of Fixed Points, Lecture Notes in Mathematics, Vol. 730, Springer, Berlin, 1979.
[30] W. Słomczyński, J. Kwapień, K. Życzkowski, Chaos 10 (2000) 180.
[31] A. Ostruszka, P. Pakoński, W. Słomczyński, K.Życzkowski, Phys. Rev. E, submitted for publication; LANL Archives, Preprint Chao-dyn/9905041.
[32] B. Derrida, A. Gervois, Y. Pomeau, Ann. Inst. Poincaré A 29 (1978) 305.
[33] B.-L. Hao, Elementary Symbolic Dynamics, World Scientific, Singapore, 1989.
[34] A. Boyarsky, P. Góra, Laws of Chaos, Birkhäuser, Boston, MA, 1997.
[35] A. Renyi, Probability Theory, North-Holland, Amsterdam, 1970.
[36] H.E. Nusse, J.A. Yorke, Physica D 36 (1989) 137.
[37] J. Jacobs, E. Ott, C. Grebogi, Physica D 108 (1997) 1.
[38] R. Haner, R. Schilling, Europhys. Lett. 8 (1989) 129.
[39] T. Tél, in: Bai-lin Hao (Ed.), STATPHYS, Vol. 19, World Scientific, Singapore, 1996.
[40] Entire special issue, Chaos 4 (1993).
[41] P. Gaspard, S.A. Rice, J. Chem. Phys. 90 (1989) 2225.
[42] C. Jung, E. Ziemniak, J. Phys. A 25 (1992) 3929.
[43] C. Jung, T. Tél, E. Ziemniak, Chaos 3 (1993) 555.
[44] E. Ziemniak, C. Jung, T. Tél, Physica D 76 (1994) 123.
[45] Á. Péntek, T. Tél, Z. Toroczkai, J. Phys. A 28 (1995) 2191.
[46] Á. Péntek, T. Tél, Z. Toroczkai, Fractals 3 (1995) 33.
[47] Á. Péntek, Z. Toroczkai, T. Tél, C. Grebogi, J. Yorke, Phys. Rev. E 51 (1995) 4076.
[48] M. Hénon, Physica D 33 (1988) 132.
[49] P.T. Boyd, S.L.W. McMillan, Phys. Rev. A 46 (1992) 6277.
[50] R.V. Jensen, Chaos 1 (1991) 101.
[51] G. Handke, Phys. Rev. A 50 (1994) R3561.
[52] S. Bleher, C. Grebogi, E. Ott, Physica D 46 (1990) 87.
[53] C. Grebogi, E. Ott, J.A. Yorke, Physica D 7 (1983) 181.
[54] Q. Chen, E. Ott, L.P. Hurd, Phys. Lett. A 156 (1991) 48.
[55] S. Hayes, C. Grebogi, E. Ott, A. Mark, Phys. Rev. Lett. 73 (1994) 1781.
[56] E. Rosa, S. Hayes, C. Grebogi, Phys. Rev. Lett. 78 (1997) 1247.
[57] E. Bollt, M. Dolnik, Phys. Rev. E 55 (1997) 6404.
[58] M. Dolnik, E. Bollt, Chaos 8 (1998) 702.
[59] E. Bollt, Y.-C. Lai, Phys. Rev. E 58 (1998) 1724.

[60] R.E. Blahut, Principles and Practice of Information Theory, Addison-Wesley, Reading, MA, 1988.

[61] I. Kan, H. Koçak, J.A. Yorke, Ann. Math. 136 (1992) 219.

[62] S. Newhouse, T. Pignataro, J. Statist. Phys. 72 (1993) 1331.

[63] P. Grassberger, Phys. Lett. A 97 (1983) 227.

[64] H.G.E. Hentschel, I. Procaccia, Physica D 8 (1983) 435.

[65] T.C. Halsey, M.H. Jensen, L.P. Kadanoff, I. Procaccia, B.I. Shraiman, Phys. Rev. A 33 (1986) 1141.

[66] B. Rückerl, C. Jung, J. Phys. A 27 (1994) 55.

[67] P. van der Schoot, M.E. Cates, Europhys. Lett. 25 (1994) 515.

[68] W. Breymann, J. Vollmer, Z. Phys. B 103 (1997) 539.